Chapter 6
Effects of Wall Roughness on Gas-particle Flows

In this chapter, a gas-particle flow in an in-line tube bank and a gas-particle flow in a two dimensional bend are numerically simulated using the Eulerian-Lagrangian model. The major objectives are to investigate the effects of wall roughness on the particle phase properties. The stochastic wall roughness model (Sommerfeld, 1992) used in this study were implemented into the FLUENT code via the User-defined subroutines. This allows the flexibility for extending the collision model to handle complex engineering flows.

6.1 Turbulent gas-particle flow over an in-line tube bank

6.1.1 Background and previous studies

A great deal of research efforts and resources have been allocated to investigate the characteristics of particle-wall collisions in gas-particle flows. Through these probing investigations, significant improvements to prolong the operational longevity of industrial devices that are constantly subjected to the rigorous bombardment of solid particles can be achieved (Tu et al., 2004). Some typical examples of such devices are heat exchanger tubes in coal combustion equipments that are widely used in chemical plants. The bombardment of coal ash particles on the heat exchanger tubes for considerable periods of time can cause significant erosion to the extent that may result in the catastrophic consequences because of continuing removal of materials from these tubes (Morsi et al., 2004).

This study presents one of the continuing series of efforts to better understand the particle-wall collision phenomenon and its contributions to the characteristics of particle phase flow field. Previously, Tu et al. (1998) measured the gas-particle flow in an in-line tube bank using the Laser-Doppler anemometry (LDA) system and compared the measurements with predictions of an Eulerian-Eulerian model. Reasonable agreements were obtained between the predicted and measured mean flow field of both gas and particle phases. The inherent weakness of the Eulerian formulation was to correctly describe the aerodynamics

drag force on the particle phase in the vicinity of a wall surface. It has demonstrated that the incident and reflected particles during the process of particle-wall collision were still far away from adequate resolution for the Eulerian-Eulerian model.

To overcome the difficulties associated with the application of the Eulerian-Eulerian approach for the particle phase, the Lagrangrian particle-tracking model is thereby revisited to study the gas-particle flows. The Eulerian-Lagrangian model considers the motion of individual particle and relevant variables along the particle trajectory. It can therefore provide rather detailed physical description of the particle behaviours in near-wall region before and after collision. The rebounding characteristic of glass particle (with diameters of 66 μm and 93 μm) impacting on the stainless steel tube bank had been investigated in Morsi et al. (2004) by using both Eulerian-Lagrangian modelling method and LDA measurement. A simple collision model was employed in which the normal and tangential restitution coefficients were respectively assumed as $e_n = -v_n^p / u_n^p = 0.9$ and $e_t = v_t^p / u_t^p = 0.9$. Tu et al. (2004) further carried out a study of particle rebounding characteristics in the gas-particle flow over a cylindrical body. The simple collision model for the Lagrangian modelling technique was also employed assuming the normal and tangential restitution coefficients set as $e_n = 0.3$ and $e_t = 0.9$. Because of the varying and arbitrary restitution coefficients that can be adopted or specified, there is a need to employ a more realistic particle-wall collision model in the context of CFD modelling. It has been known that several physical parameters govern the particle-wall collision process. Among these parameters are the particle incident velocity, particle initial angular velocity, incident angle, diameter and shape of the particle as well as its material properties. Other parameters such as the surface characteristics and roughness can also contribute to significantly influence the particle impacting on and rebounding away from the wall surface (Li et al., 2000; Sommerfeld, 1992). Primarily, the absence of any dependence of the particle rebounding characteristics on physical parameters such as particle incident velocity, particle initial angular velocity and the surface roughness presents additional considerations of which are crucial to incorporate within the collision model.

In order to obtain more accurate description of particle-wall collision phenomenon, this study employed an algebraic particle-wall collision model developed by Brach and Dunn (1992 and 1998). Based on Newton's laws in the form of impulse and momentum (Brach

et al., 2000), this algebraic collision model has the ability to deal with oblique collision and to calculate the particle angular velocities (Brach and Dunn, 1998). Another distinguished feature of this model is that it can account for the particle deposition on the surfaces by introducing a critical or capture velocity. When the particle incident velocity is lower than the critical velocity, the particle is assumed to deposit on the surface.

For particles with diameters in the range of 1 μm ~ 100 μm and relatively high incident velocities, the particle rebound velocities follow the same trend, i.e. the restitution coefficients are almost constant when the particle incident velocities vary. Nonetheless, when the incident velocities become relatively low (below ~ 10 m/s), the rebound velocities decrease remarkably. In other words, the normal restitution coefficients decline dramatically when the incident velocities reduce (Brach and Dunn, 1992). Thus, the influence from the incident velocities onto the restitution coefficients is not negligible. This algebraic particle-wall collision model has been developed to account for this phenomenon by formulating the overall restitution coefficient as a function of the incident velocity.

The particle-wall collision model should also consider the wall roughness and the resulting stochastic nature of the process, since experimental investigations (Grand and Tabakoff, 1975; Govan et al., 1989) have found that the particle restitution coefficient is subject to some scatter due to wall roughness and non-spherical particles (Sommerfeld, 1992). Several models had been proposed to account for the effect of ‘wall roughness’ (Matsumoto and Saito, 1970; Tsuji et al., 1987; Sommerfeld, 1992). One notable finding whilst employing a traditional particle-wall collision model without incorporating wall-roughness was that particles eventually deposited at the bottom of the channel, which had been demonstrated in the numerical study of gas-particle flow in the horizontal channel by Tsuji et al. (1987). That appeared to be inconsistent with experimental observation since it clearly showed that the particles continued to be suspended in the free-stream flow. When the “virtual wall model” was applied to account for the wall roughness, the particles suspended and constituted a steady flow. In the present study, a stochastic approach developed by Sommerfeld (1992) was adopted to take into consideration of the wall roughness effect.

6.1.2 Numerical procedure

The generic CFD code, FLUENT, was utilised to predict the continuum gas phase of the velocity profiles under steady-state conditions through solutions of the conservation of mass and momentum. The air phase turbulence was handled by the RNG based k-ε model (Yakhot and Orzag, 1986). Because of the nature of its derivation and fundamental development, the RNG k-ε model is expected to be applicable to a wider range of flow situation than the standard k-ε model and has been employed to predict the gas flow over single tube (Lee et al., 2000) and over tube bank (Morsi et al., 2004). The significance of the inclusion of this term is its responsiveness towards the effects of rapid rate strain and streamlines curvature, which cannot be properly represented by the standard k-ε turbulence model. According to the RNG theory (Yakhot and Orzag, 1986), the constants in the turbulent transport equations are given by $\sigma_\kappa = 0.718$, $\sigma_\varepsilon = 0.718$, $C_\mu = 0.0845$, $C_{\varepsilon 1} = 1.42$ and $C_{\varepsilon 2} = 1.68$ respectively. The constants k, l, a, b and u_c (capture velocity or critical velocity) are to be obtained through experiments. In this study, R_1, ρ_1 and e were calculated based on the constants of Ag-coated glass particle impacting on stainless steel surface (Brach and Dunn, 1998), i.e. k = 272.0, l = 1.74, a = 1.0, b = 1.0 and u_c = -0.4 m/s. Figure 6.1 shows the values of R_1, ρ_1 and e as the function of normal incident velocities. The negative capture velocity may result from insufficient low-velocity data or from variations due to uncontrolled factors. Nevertheless, Brach and Dunn (1998) showed that the likelihood for such a condition was extremely low.

The algebraic particle-wall collision model (Brach and Dunn, 1992 and 1998) is used to account for the particle-wall collision procedure. A stochastic approach has been developed by Sommerfeld (1992) to take the wall roughness effect into consideration. Here, the incident angle θ' comprises of the particle incident angle θ and a stochastic contribution due to the wall roughness, $\theta' = \theta + \Delta\gamma\xi$. Here, ξ is a Gaussian random variable with mean of 0 and a standard deviation of 1. The value of $\Delta\gamma$ is determined through experiment. In this study, the wall roughness $\Delta\gamma$ of 5.3° was used. This value was obtained for 100 μm glass particles impacting on steel surface by Sommerfeld and Huber (1999). More details about the algebraic particle-wall collision model (Brach and Dunn, 1992 and 1998) and the stochastic wall roughness model (Sommerfeld, 1992) can be found in Chapter 3.3.

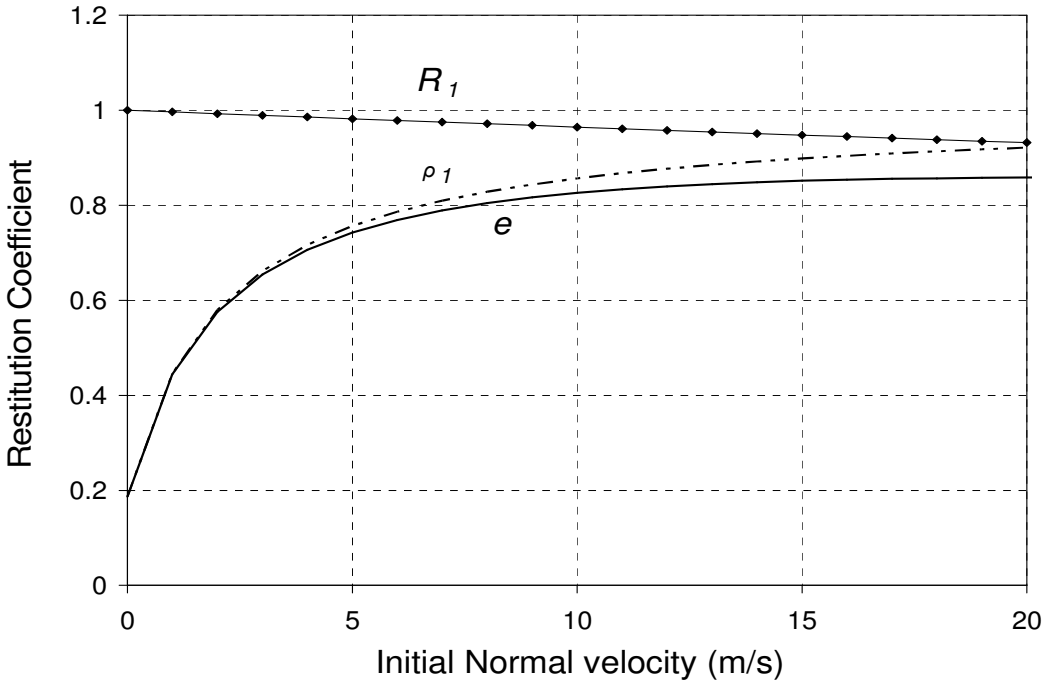

Figure 6.1 The dependence of R_1, ρ_1 and e on the normal incident velocities.

The Non-Equilibrium wall function was employed for the gas phase flow because of its capability to better handle complex flows where the mean flow and turbulence are subjected to severe pressure gradients and rapid change, such as separation, reattachment and impingement. The governing transport equations were discretised using the finite-volume approach. The QUICK scheme was used to approximate the convective terms while second order accurate central differencing scheme is adopted for the diffusion terms. The pressure-velocity coupling was realized through the SIMPLE method. The convergence criteria for the gas phase properties were 10^{-5}. The governing equations for the gas phase were initially solved towards steady state. The numerical exercise was performed in a two-dimensional environment because only 2D representative measurements are available. The Lagrangian solution for the particle phase was thereafter achieved by the injection of particles into the bulk gas flow where the trajectories of each particle were determined from the steady state gas phase results.

6.1.3 Grid independence test

The particle-gas flows over an in-line tube bank were predicted by the Eulerian-Lagrangian model combining with the algebraic particle-wall collision model (Brach and

Dunn, 1992 and 1998) and the stochastic wall roughness model (Sommerfeld, 1992). Glass articles (material density 2990 kg/m^3) with corresponding diameters of 1 μm, 15 μm and 93 μm were simulated under the flow condition with the Reynolds number of 18667 (based on the tube diameter D=0.025m).

Figure 6.2(a) shows the two-dimensional computational domain with a size of 750 mm × 100 mm comprising of six tubes and twelve half tubes respectively. The gas inlet velocity is 11.2 m/s with a uniform profile at the location x = -50 mm. The outlet boundary is 275mm (11D) downstream of the sixth tube. Symmetrical conditions are assumed at the top and bottom of the computational domain. These are slightly different from the experimental observation for the particle phase due to the gravity acting to the direction perpendicular to the flow.

The grid independence was checked by comparing the computed gas phase velocity and turbulence intensity profiles with measurements. All the comparison and validation were carried out in the region shown in Figure 6.2(b) (from 0 mm to 105 mm in x direction and from 0 mm to 25 mm in y direction). Three mesh densities were generated for computational domain –67858, 87370 and 108797 quadrilateral elements. Figure 6.2(c) illustrates part of the mesh of 108797 cells.

Figure 6.3(a) shows the comparison between the measured and predicted streamwise gas velocity profiles using three different mesh schemes at locations x = 15, 30, 45, 60, 75, 90 and 105 mm. The fine mesh density if 108797 grid points and medium mesh density of 87370 grid points yielded almost identical solutions to the measured data (within 8 %) except with an under-prediction up to 53 % in the wake region (x = 45 mm, y = 1 mm) and an over-prediction of 36 % at the location of x = 105 mm, y = 15 mm. The predictions of streamwise gas turbulence intensities using the different mesh densities comparing with the measurements are presented in Figure 6.3(b). All the three mesh densities predicted very similar results that were in close agreement with the measurements (within 5 %) up to x = 45 mm but deviated at the locations of x = 60 mm, y=10 mm (as high as 64 %), x = 75 mm, y =1 mm (as high as 58%) , x = 90 mm, y = 15 mm (as high as 65%). From the consideration of accuracy, simulation results presented below were hereafter obtained using the fine mesh density of 108797 grid points.

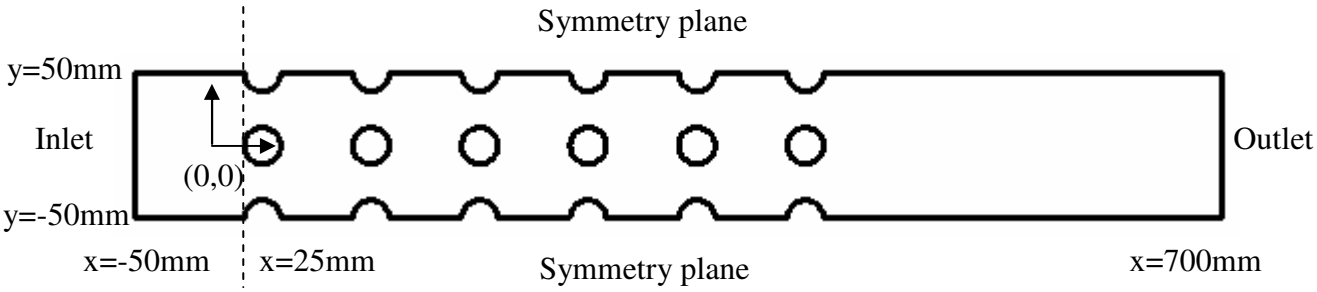

(a)

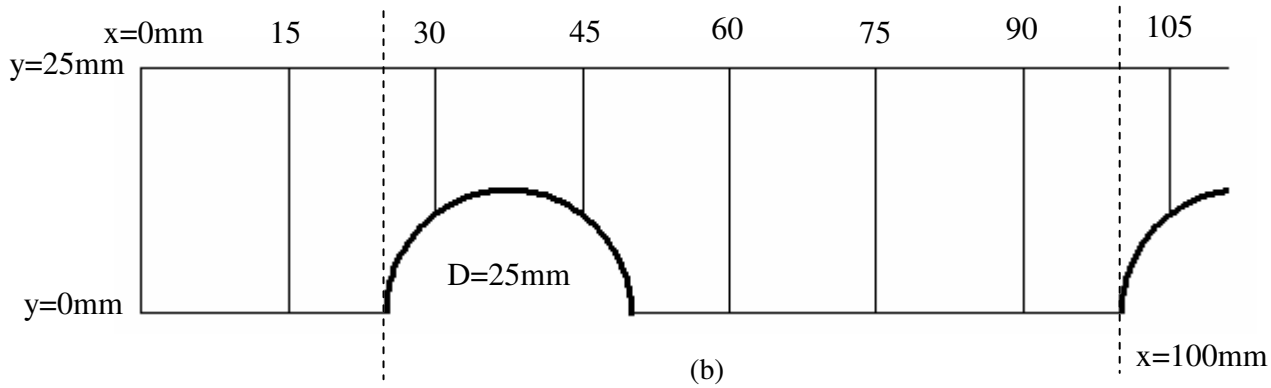

(b)

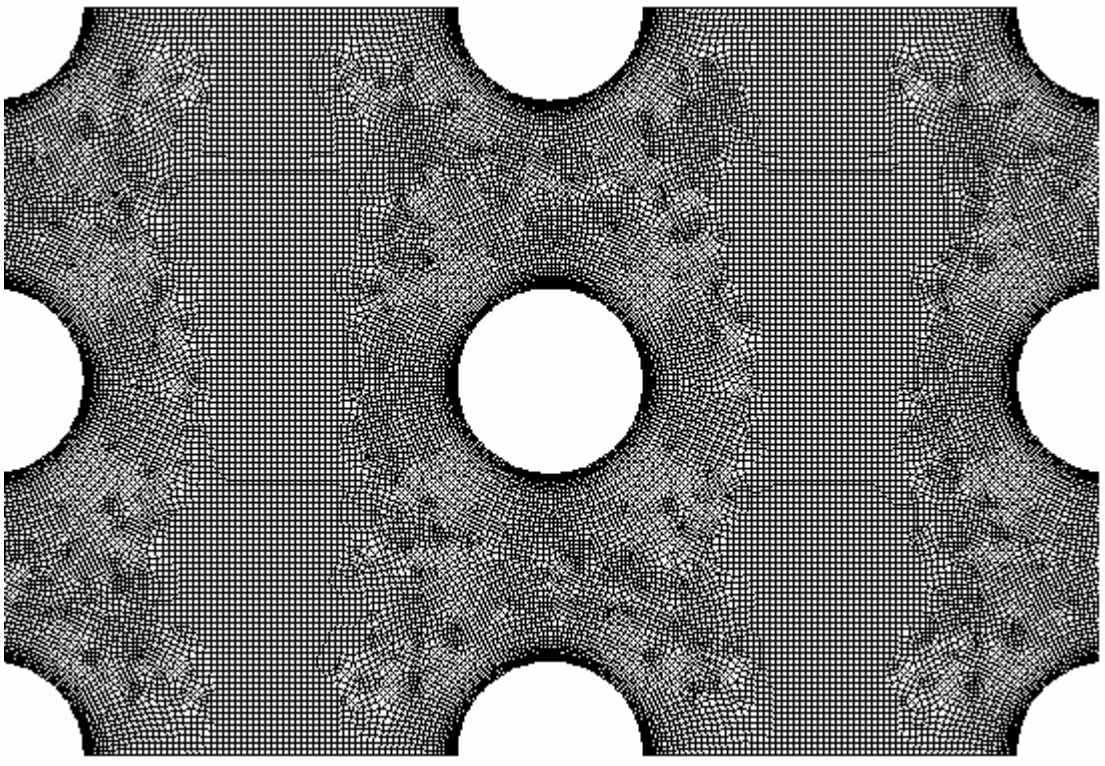

(c)

Figure 6.2 (a) Computational domain, (b) Region of comparison between prediction and measurement, (c) Part of mesh density 108797.

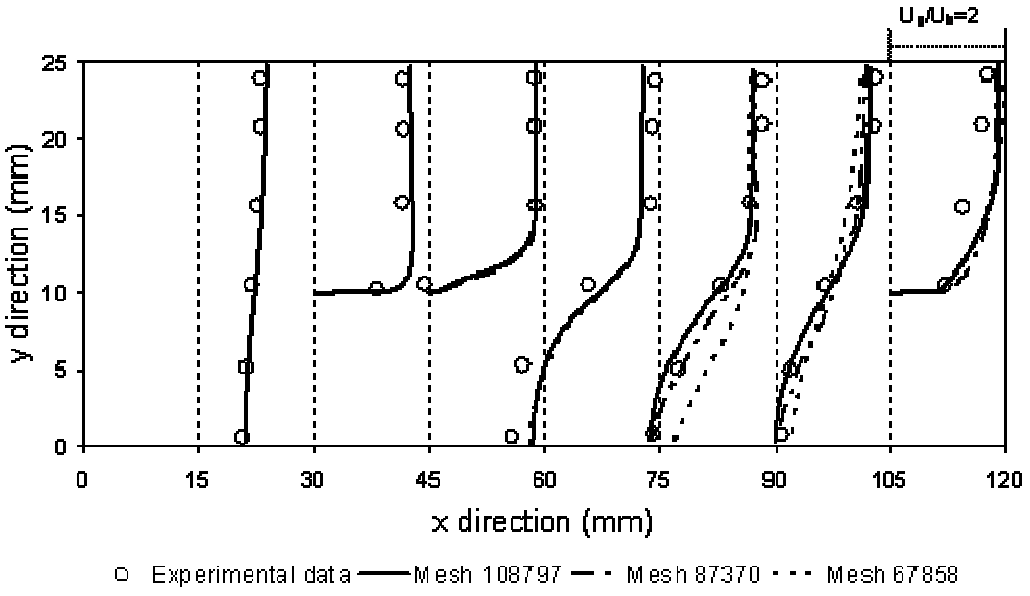

(a)

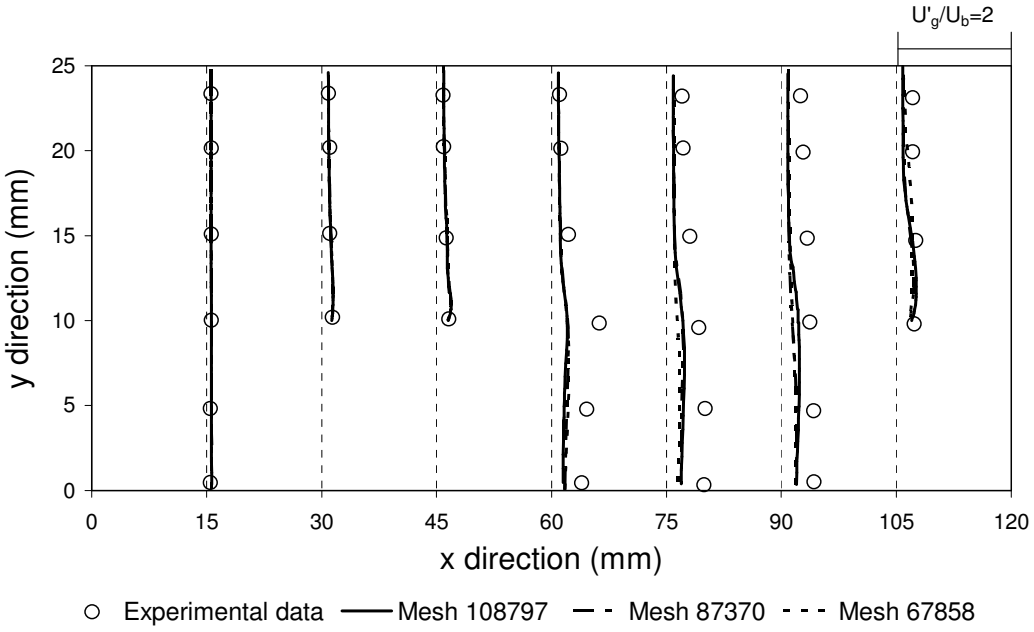

(b)

Figure 6.3 Comparisons predictions of gas phase with experimental data: (a) streamwise velocity profiles, (b) turbulence intensity.

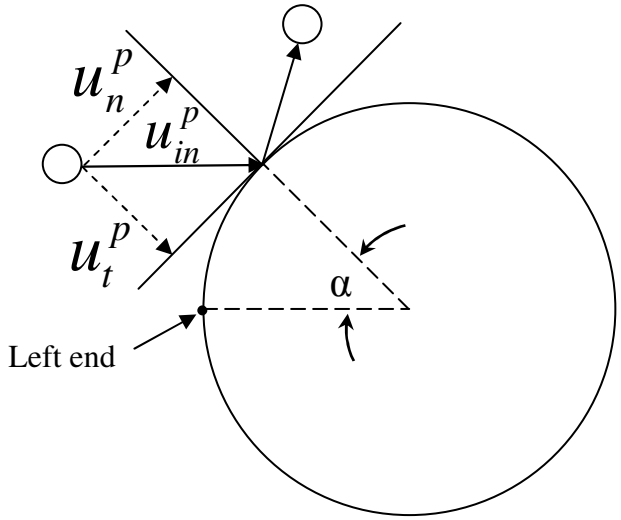

α angular location of collision (degree)

Error! Objects cannot be created from editing field codes.

normal incident velocity

(a)

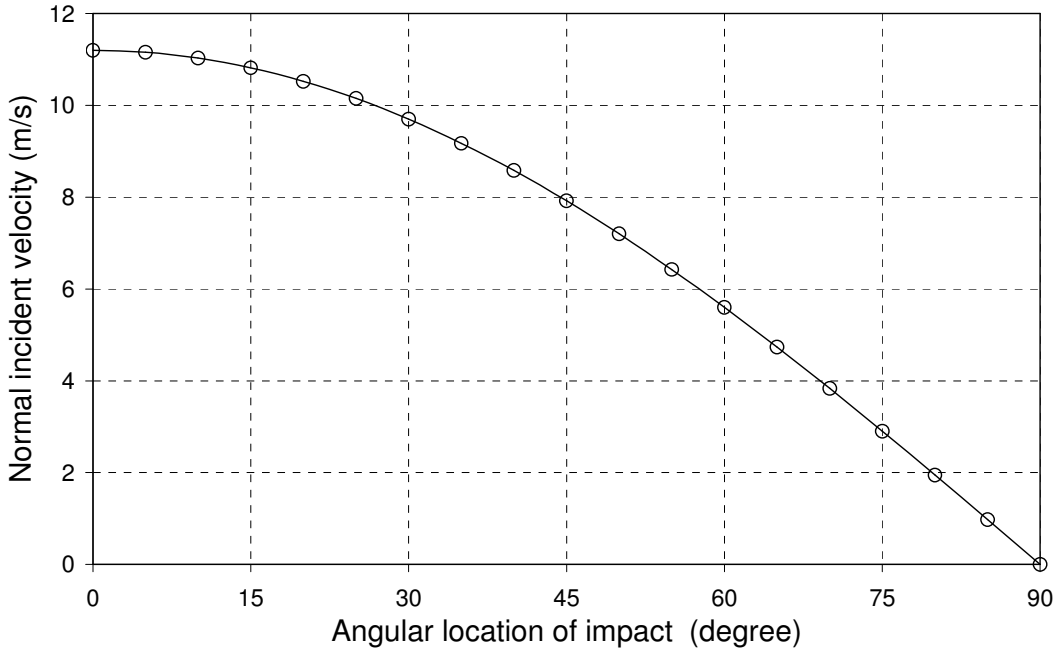

(b)

Figure 6.4 (a) The velocity and angle notations for the particle colliding on the tube, (b) the particle normal incident velocity of different angular location.

6.1.4 Particle phase simulation validation

The velocities and angle notations for the particle colliding on the tube are given in Figure 6.4(a). Figure 6.4(b) shows the normal incident velocities of particles at different angular location. For the numerical validation, 50,000 particles were injected from 50 uniformly distributed points across the line x = 0 mm and they were individually tracked within the in-line tube bank. A pre-processor code was developed to assign an initial velocity to individual particle. Firstly, the local particle velocities and turbulence intensities at every injection point were obtained by interpolating the experimental results. Then, every particle was assigned a normal distribution random velocity that had a mean with the value of local mean particle velocity and a standard deviation with value of local particle turbulence intensity. The annular velocities for the particles at inlet were assumed to be zero as no experimental measurement was made available.

The predicted velocities and turbulence intensities of particles with uniform diameter of 93 μm were validated against the experimental data of Tu et al. (1998). Figure 6.5(a) presents the comparison for the calculated 93 μm particle velocity. The predictions and measurements showed good agreement (within 20 %). Figure 6.5(b) illustrates the comparison of 93 μm particle fluctuating velocity. An over-prediction of the particle velocity as high as 45 % was attained at the top entrance (x = 0 mm, y = 23 mm). An under-prediction of the particle velocity was obtained at the location x = 60 mm, y = 10 mm. Close agreement was nonetheless found in other locations within 15 %.

6.1.5 The effects of wall roughness on particle trajectories

As aforementioned, the particle-wall collision model should account for the wall roughness effect. The influence of wall roughness on the particle rebounding characteristics was investigated. Figure 6.6(a) illustrates the trajectories of forty 93 μm particles released at the location of (-0.04, 0.0) without the wall roughness model. Most particles rebounding from the upstream middle tube at first collision were seen to collide with the succeeding top and bottom tubes downstream. Some of these particles were found to collide with the central tube in-line between the top and bottom tubes. This recurring particle rebounding characteristics were also similarly experienced further downstream of the subsequent in-

line tube bank. Nonetheless, when the effect of wall roughness was taken into consideration, the behaviours of particles were markedly different from those without accounting for the wall roughness. Figure 6.6(b) clearly indicates that the wall roughness had a considerable influence on the particles rebounding behaviours. Particles were found to be more suspended with the flow stream missing in some circumstance the central tube in the second in-line tube bank arrangement following the first collision at the upstream middle tube.

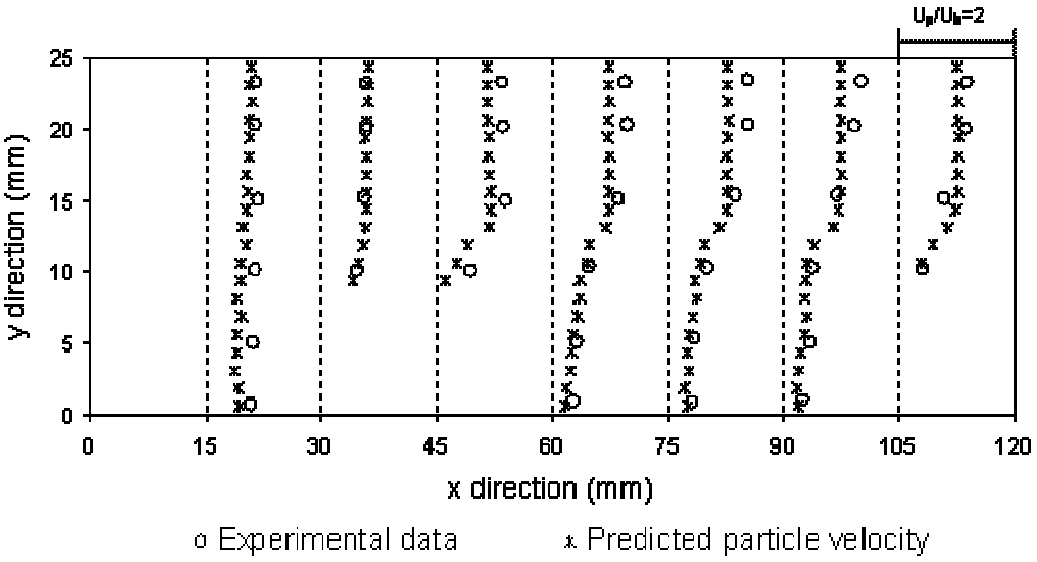

(a)

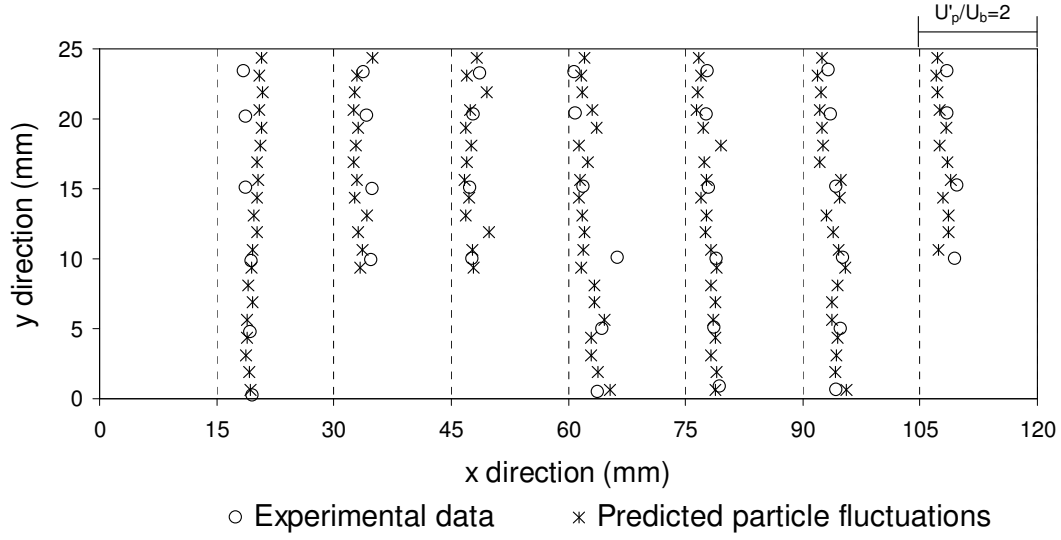

(b)

Figure 6.5 Comparisons of predictions of 93 μm particles with experimental data: (a) streamwise velocity, (b) turbulence intensity.

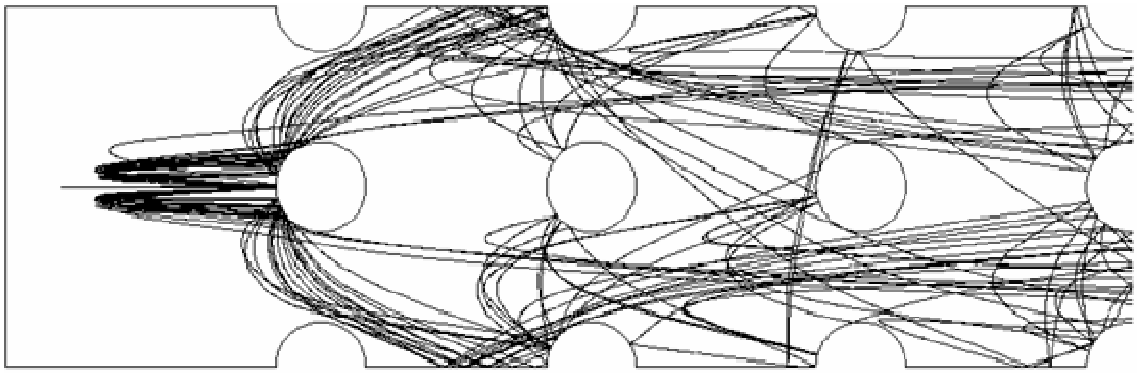

(a)

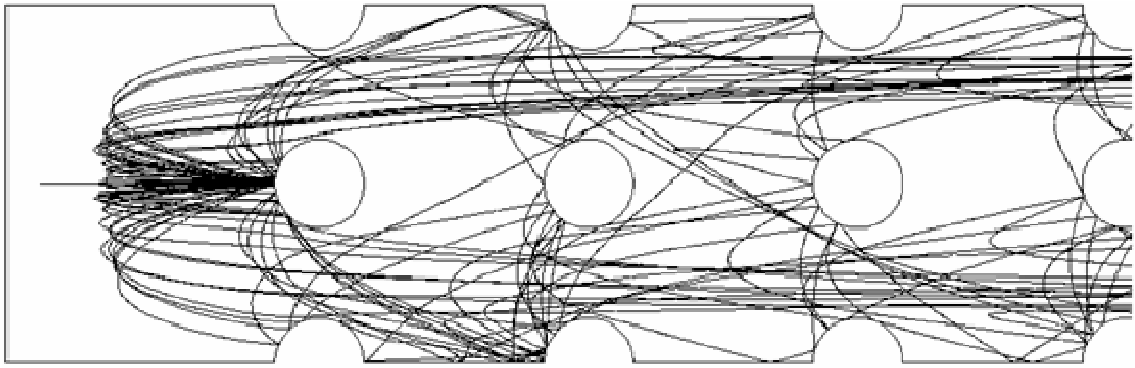

(b)

Figure 6.6 Computed trajectories for 93 μm particles: (a) without roughness model, (b) with roughness model.

The wall roughness can considerably influence the mean particle phase velocities for large particles. In their experimental studies of the gas-particle flows in a channel flow, Kussin and Sommerfeld (2002) found that when the wall roughness is substantially increased, the stream wise mean particle velocity can be considerably reduced, which is a consequence of the average increase in momentum loss for the particle phase.

For many coal combustion equipments in chemical plant, the heat exchanger tubes subject to prolong bombardment of particle exposes themselves to significant erosion problem. Erosion damage in tubes has been ascertained in many published literatures that it depends primarily on the characteristics of the particle incident velocity, incident angle and particle collision frequency (Morsi et al., 2004). The effect of wall roughness on the particle collision frequency distribution was investigated by injecting 50,000 particles (93 μm) with uniform inlet velocity of 11.2m. Herein, the particle collision frequency was defined to be the ratio of the total number of particle colliding on different parts of tubes to the

number of 500. Figure 6.7 shows the particle collision frequency of the second middle tube with and without wall roughness model. It is clearly seen that the wall roughness has considerably altered the distribution of particle collision frequency.

Generally, the wall roughness model should therefore be included in the particle-wall collision model to provide a more realistic description of the particle-wall collision phenomenon and further more accurate erosion rate prediction.

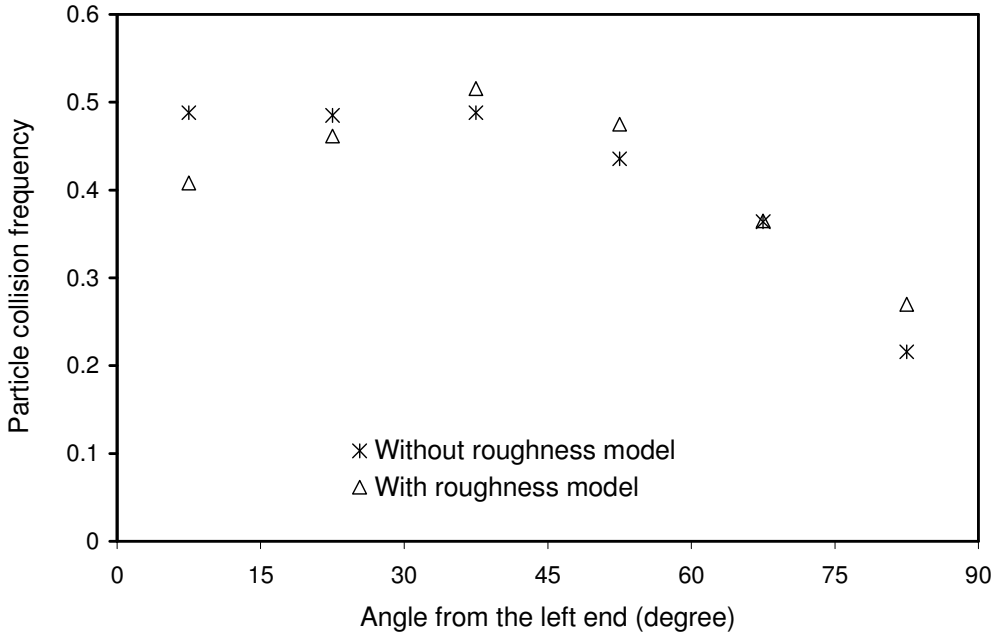

Figure 6.7 Particle collision frequency distribution on the second middle tube.

6.1.6 The effects of particle-wall collision on particle phase flow

The flow patterns of particles with different sizes are presented in Figure 6.8. In Figure 6.8(a), the trajectories of larger particles (93 μm) in the in-line tube bank showed considerable particles rebounding from the top, middle and bottom tubes along the first in-line tube bank arrangement at initial collision; the same vigorous behavior was also repeated in subsequent tubes downstream. For smaller particles (15 μm) in Figure 6.8(b), since the particles possessed lower inertia and gained less momentum to overcome the drag of the fluid, a significant reduction of the particles rebounding from the tube wall surfaces was predicted. Following the initial collision at the top, middle and bottom tubes along the first in-line tube bank arrangement, the particles were found to be totally suspended across

the second and third in-line tubes before colliding again the top and bottom tubes at exit. For even lighter particles (1 μm), the gas motion and turbulent dispersion dictated the particle motion and the particles closely followed the gas flow (see Figure 6.8(c)). Some particles were observed to be entrained into the wake regions behind the tubes causing very few particles to collide indicating that the influence of particle-wall collision could be neglected.

For the case of 93 μm particle, the Stokes number was evaluated to be 31; a value much greater than unity. The influence from the fluid-phase fluctuations onto the 93 μm particles was found to be negligible. Rather, the particle phase velocity fluctuations were determined by the particle-wall collisions.

A "CFD experiment" was conducted to investigate the influence of particle-wall collisions on the particle fluctuations for different particle sizes. 50,000 particles with diameter of 93 μm were injected from inlet with a uniform streamwise velocity 11.2 m/s. In other words, the stream wise velocity fluctuations for the inlet particles were set to be zero. The particle velocity fluctuations in the in-line tube bank were obtained by two different assumptions of the particle-wall interactions. For the first assumption, particles were assumed to be trapped on the surface when reaching the tubes while for the second, the particle-wall collision model (Brach and Dunn, 1992) was adopted meaning that particles were rebounding from the circumferential wall tube surfaces. Figure 6.9 illustrates the distribution of the turbulent intensity for the two different particle diameters at various axial locations. As shown in Figure 6.9(a), the particle velocity fluctuations for the particle-trapping case yielded almost zero turbulence intensities from x = 15 mm to x =105 mm, while considerably higher particle velocity fluctuations were found for the particle-rebounding case. This clearly indicated that the particle-wall collision has a significant influence on the particle phase velocity fluctuations for the larger size particles, which was also confirmed through the experimental studies of Kussin and Sommerfeld (2002). Kussin and Sommerfeld (2002) reported that when the wall roughness was increased, the components of particle mean fluctuating velocity for large particles (about 100 μm) were considerably enhanced by the irregular wall-bouncing process.

Similar "CFD experiment" was also performed for the 1 μm particles and the results are given in Figure 6.9(b). The close predictions of the two particle-wall assumptions

suggested that the particle-wall collision has no effect on the particle velocity fluctuations for small particles.

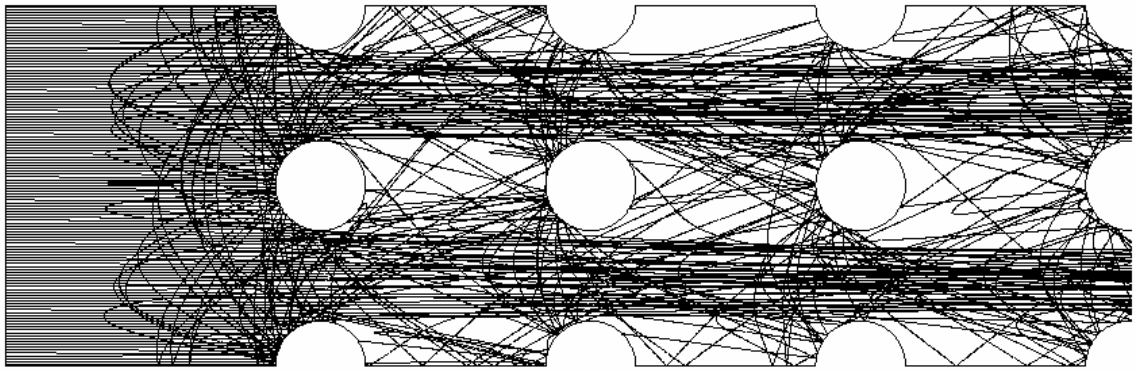

(a)

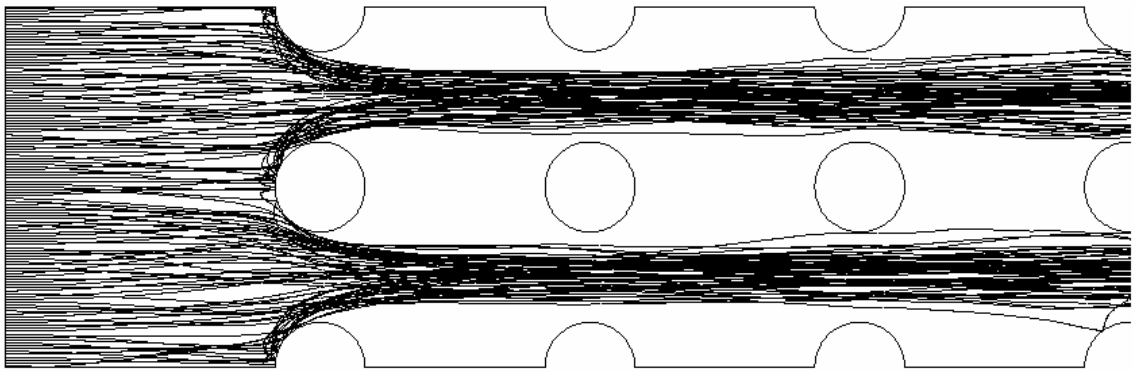

(b)

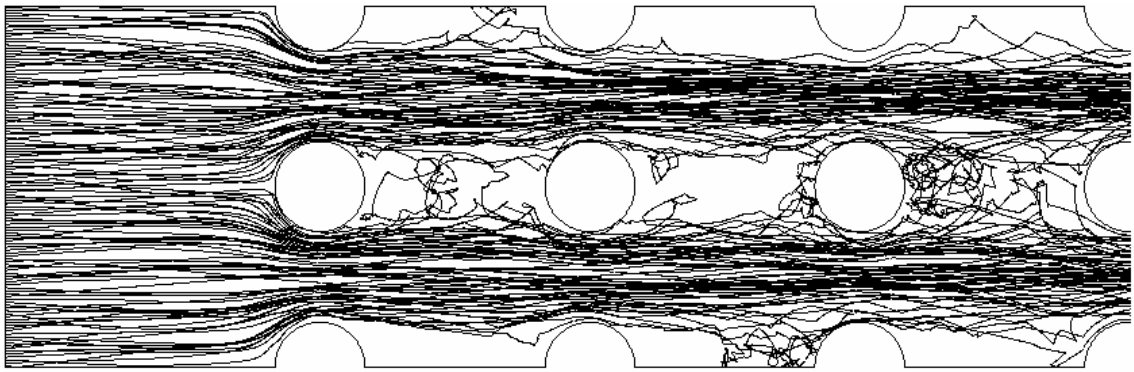

(c)

Figure 6.8 Computed particle trajectories: (a) 93 μm, (b) 15 μm, (c) 1 μm.

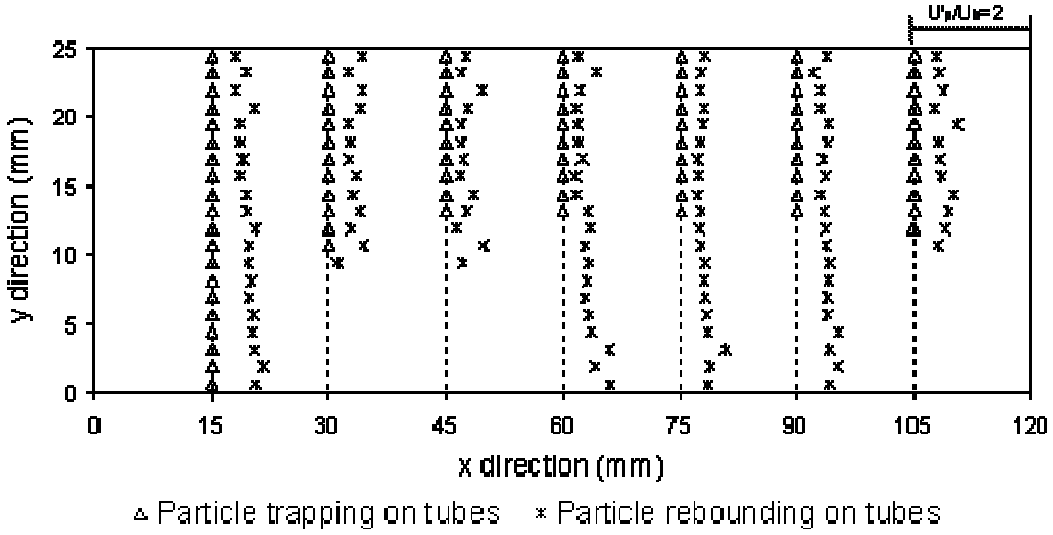

(a)

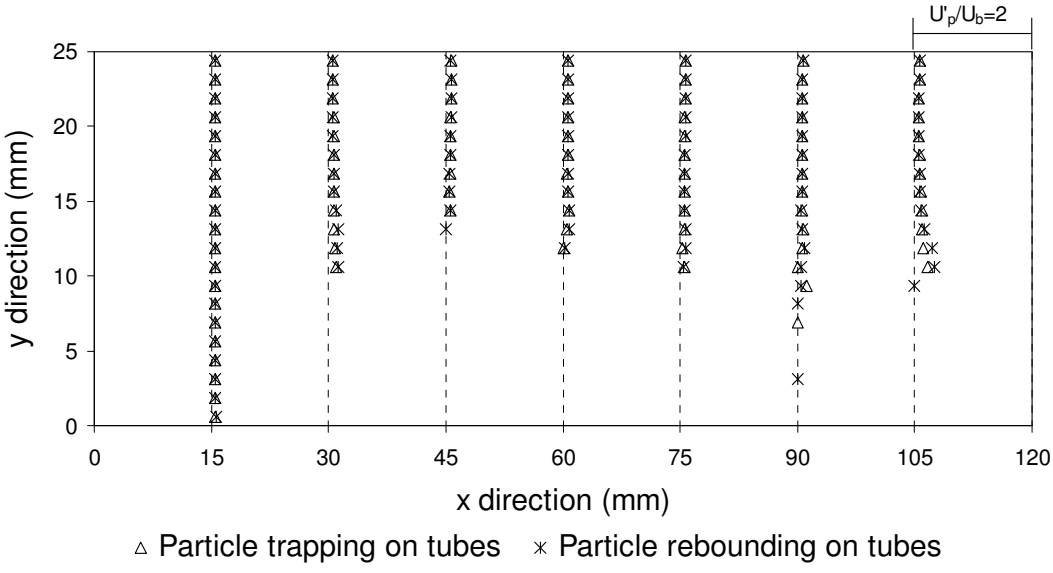

(b)

Figure 6.9 Comparisons of turbulence intensity for particle trapping and rebounding: (a) 93 μm particles, (b) 1 μm particles.

Figure 6.10 illustrates the stream wise mean velocities for the gas, 1 μm particles and 93 μm particles. The smaller particles (1 μm) behaved very similar to those of the gas flow. At x = 30 mm, the momentum of the gas and lighter particles (1 μm) was significantly increased with the velocity profiles shifted towards the right. The increase of the velocity profiles of the large particles (93 μm) was marginal due to higher inertia. Notably also for the 1 μm particles, the Eulerian-Lagrangian model predicted a particle-free zone in the wake regions behind the cylindrical tubes.

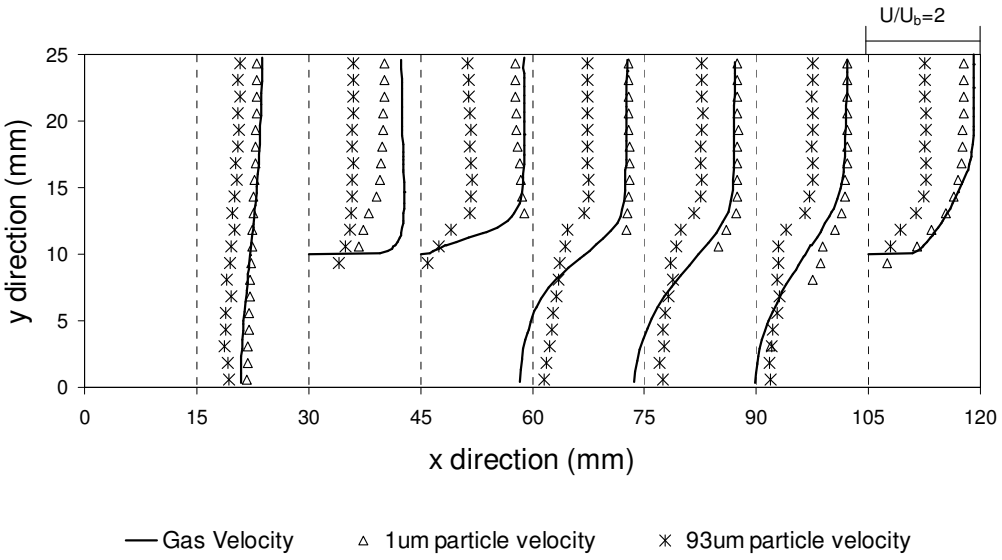

Figure 6.10 Predicted mean streamwise velocity for gas, 1 μm and 93 μm particles.

6.1.7 Summary

The physical behavior of a dilute gas-particle flow along an in-line tube bank was numerically investigated via a Lagrangian particle-tracking model. An algebraic particle-wall collision model developed by Brach and Dunn (1992 and 1998) was utilized to account for the particle-wall interaction and a stochastic model (Sommerfeld, 1992) was adopted to take wall roughness effect into consideration.

The predictions of the mean flow fields for both gas and particle phase were validated against experimental data of Tu et al. (1998). Close agreements were achieved between the predictions of mean velocity and experimental data for gas phase (agreement within 8% except some locations in the wake and exit regions). The predicted gas phase turbulence was lower (up to 65%) than the measurement in the region after the first cylinder. These indicated that more accurate turbulence models such as Large Eddy simulation (LES) models may be required to appropriately resolve the complex air flows in the tube bank. The predicted velocities of 93 μm particle were in good agreement with the experimental results (within 20 % despite of the local large discrepancy of gas phase fluctuation after the first cylinder). This was due to the fact that 93 μm particles have sufficient inertial and did not follow the gas phase fluctuations. Close agreement were also found for the particle phase fluctuating velocities.

A substantial amount of work was taken in this study to elucidate further the understanding of the effect of wall roughness on particle phase flow field. Through a "CFD experiment", it was established that the wall roughness considerably altered the rebounding behaviours of large particles, and consequently affected their motions downstream and particle collision frequency distribution on tubes. This suggested that the particle-wall collision model should account for the effect of wall roughness in order to provide a more realistic description of the particle-wall collision phenomenon.

The influence of particle-wall collisions on the particle fluctuations for different particle sizes was also investigated. The numerical results confirmed that the particle fluctuations were mainly determined through the particle-wall collisions for large particles, but not by the gas phase fluctuations. For small particles, the influence of particle-wall collision on the particle phase fluctuations was found to be negligible.

6.2 The effects of wall roughness on a gas-particle flow in a 2D 90° bend

6.2.1 Background

As aforementioned, the wall surface roughness is one of the physical parameters that govern the particle-wall collision process and the wall collision frequency. Sommerfeld and Huber (1999) measured the gas-particle flows in a horizontal channel using particle tracking velocimetry. They found that wall roughness considerably alters the particle rebound behavior and on average causes a re-dispersion of the particle by reducing the gravitational settling. Another contribution to this work was the development and validation of a stochastic wall roughness distribution model that takes into consideration the so-called shadow effect for small particle incident angles. It was demonstrated that particles may not hit the lee side of a roughness structure when the absolute value of the negative inclination angle $|\gamma_|$ becomes larger than the impact angle Sommerfeld and Huber (1999). This results in a higher probability for the particle to hit the luff side, effectively shifting the probability distribution function of the effective roughness angle towards positive values. Later, Kussin and Sommerfeld (2002) conducted detailed measurements of gas-particle horizontal channel flows using glass particles with diameters from 60 μm to 1000 μm and two stainless steel walls with different degrees of wall

roughness. It was found that irregular particle-wall collision due to the roughness enhances the transverse dispersion of the particles across the channel and that the wall collision frequency is increased due to a reduction in the mean free path. The wall roughness was also found to decrease the particle mean velocity that is associated with a higher momentum loss in the particle phase while increasing both the streamwise and transverse fluctuating velocities. The effects of wall roughness on particle velocities in a fully developed downward channel flow in air was experimentally investigated by Benson et al. (2005), employing a laser Doppler anemometer (LDA) system. Similar to the studies by Kussin and Sommerfeld (2002), the wall roughness was found to substantially reduce the streamwise particle velocities causing the particles to be uniformly distributed across the channel after wall collision. The wall roughness also increases the particle fluctuating velocities by nearly 100% near the channel centerplane. Using a stochastic wall roughness model similar to that of Sommerfeld and Huber (1999), Squires and Simonin (2006) numerically studied the particle phase properties in a gas-particle channel flow with three wall roughness angles, 0° (smooth wall), 2.5° and 5°. The most pronounced effect of wall roughness was found on the wall-normal component of the particle velocity (the transverse particle velocity). The streamwise particle velocity variance was increased, while the transverse particle fluctuating velocity was less sensitive to the wall roughness.

The main focus of this paper is to numerically investigate the effects of wall roughness on the particle-wall collision phenomenon and to extend these ideas to further characteristise the particle phase flow in a two-dimensional (2D) 90-degree bend. This study employed the Lagrangian model, while including a particle-wall collision model and a stochastic wall roughness model (Sommerfeld and Huber, 1999) to study the effects of wall roughness on the particle phase flow field.

6.2.2 Numerical procedure

The air phase turbulence was handled by the RNG k-ε model and the Non-Equilibrium wall function was employed for the gas phase flow. The governing transport equations were discretised using the finite-volume approach and the QUICK scheme was used to approximate the convective terms while the second order accurate central difference scheme is adopted for the diffusion terms. The pressure-velocity coupling was realized

through the SIMPLE method and the convergence criteria for the gas phase properties were assumed to have been met when the iteration residuals had reduced by five orders of magnitude.

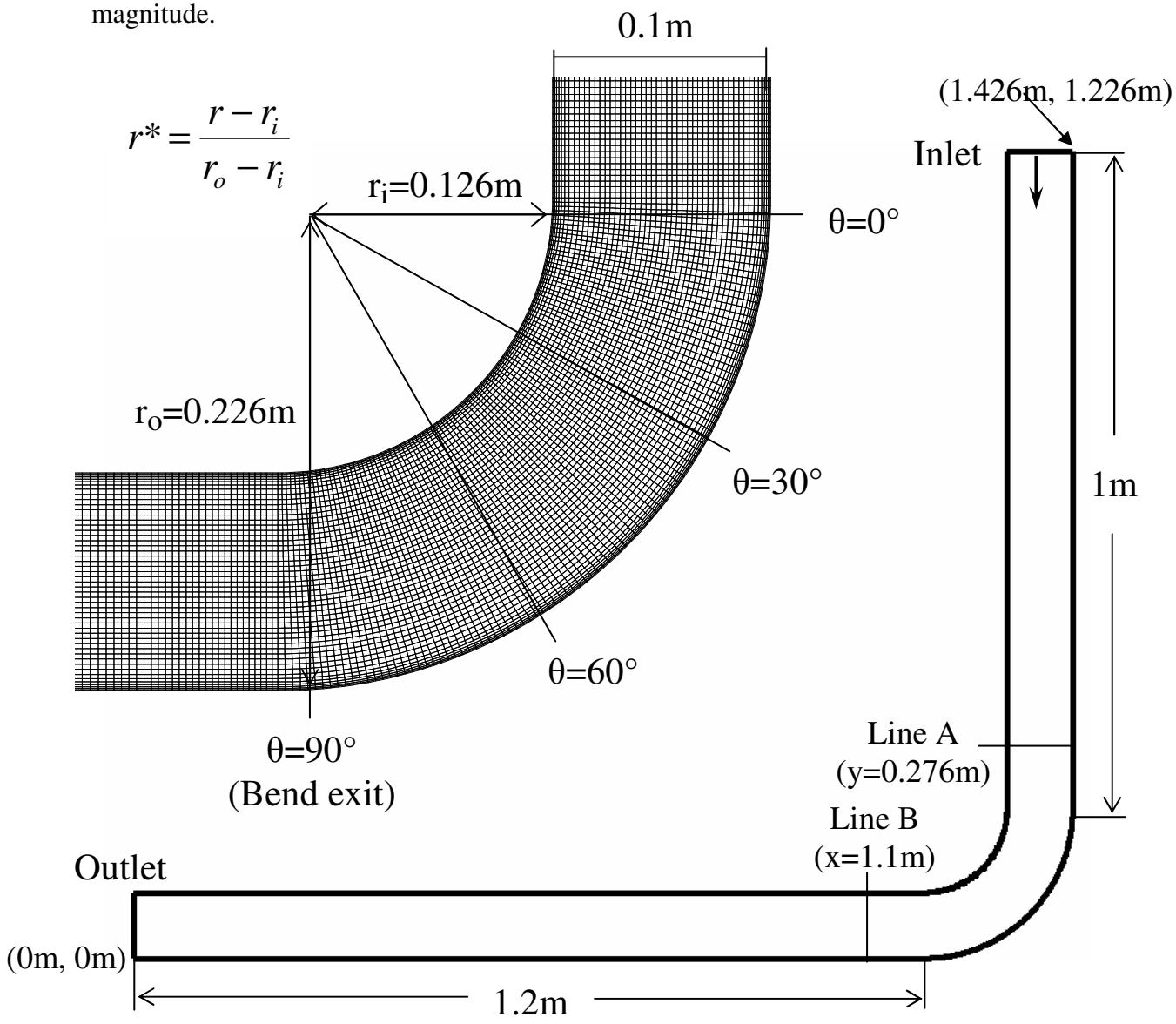

Figure 6.11 Computational domain and grids of the two-dimensional 90-degree bend.

The governing equations for the gas phase were initially solved towards steady state. The Lagrangian solution for the particle phase was thereafter achieved by the injection of particles into the bulk gas flow where the trajectories of each particle were determined from the steady state gas phase results. The main focus of this study is the effects of wall roughness on the particle phase flow field therefore, the volume fraction of particle phase was not considered and one way coupling was used. For gas-particle flows in bends, the secondary flow and side walls may impose significant influence on particle phase properties such as the particle number density (particle concentration) distribution, particle

mean velocities and particle fluctuating velocity. In order to analyze the effect of the wall roughness on particle phase field independent of the effects from the secondary flow and side wall, the current study was simulated in a two-dimensional (2-D) bend. For the same reason of simplicity, particles were assumed to be spherical and mono-sized.

Figure 6.11 shows the computational domain where the inlet begins 1 m upstream from the bend entrance and extends 1.2 m downstream from the bend exit. The bend has an inner radius (r_i) of 0. 126 m and an outer radius (r_o) of 0.226 m for the outer wall. The results were plotted against a non-dimensional wall distance $r^* = \frac{r - r_i}{r_o - r_i}$. Within the 1m long channel before the bend, 380 (in the streamwise direction) × 58 (in the transverse direction) grid points have been allocated. In the bend, the mesh is with 168 grid points in the streamwise direction and 58 grid points in the transverse direction. The 1.2m long channel after the bend has a 450 (in the streamwise direction) × 58 (in the lateral direction) grid mesh. Grid independence was checked by refining the mesh system by a mesh density of 1122 (in the streamwise direction) × 68 (in the transverse direction) grid points. Part of the grid mesh is illustrated in Figure 6.11.

The computational domain is the same as the case in Chapter 4.2 but is two dimensional. Note that the flow condition now useed an inlet velocity of 10 m/s (52 m/s in Chapter 4.2) which was more likely to be found in real engineering applications. As well, in the current study, glass particles (density is 2990 kg/m^3) with corresponding diameters of 100 μm were simulated.

6.2.3 The effects of wall-roughness on particle trajectories

The influence of wall roughness on the particle trajectories was firstly investigated by tracking 25 particles (100 μm) released from a point location at (1.376, 0.13). For qualitative purposes only a small number of particles are used as this allows particle tracking to be performed graphically without smearing of the results due to the overloading of lines associated with a large number of particles being graphically tracked. Figure 6.12 (a) illustrates the particle trajectories with 0° wall roughness angle. All the particles rebounding from the first collision followed very similar trajectories which consequently

produced a narrow secondary collision zone. The centre of this secondary collision zone is located about 0.3 D after the bend (x =1.17 m). When the wall roughness angle was increased, the behaviours of particles were markedly different. The particles were observed to rebound in many directions caused by an increase in the randomness from the rebounding of a rougher wall surface. A wider dispersion of particles was observed, leading to a significant increase in the second collision zone length. An increase of almost 4 times for the case of a 2.5° roughness angle was found in Figure 6.12(b), while an increase of 10 times was found for 5° roughness angle in Figure 6.12(c). A closer investigation for the 5° roughness angle, revealed that the secondary collision zone contained more particles impacting to the left of x=1.17m, which is the secondary collision zone location for 0° roughness. It should be noted that there exists a significant contribution from the particles inertia on the particle trajectory after the first collision. The increase in wall roughness causes a wider re-dispersion of particles, and thus this new trajectory, coupled with a high inertia results in the negligible influences from the bulk fluid. This allows the particles to travel further to the left, causing a wider secondary collision zone.

In Figure 6.12(a), the small deviation of particle trajectories after the first collision is attributed to the gas phase turbulence. For the case of 100 μm particle, the Stokes number is equal to 9 (based on characteristic length L_s = D =0.1 m and the characteristic velocity U_b = 10 m/s), much greater than unity. Therefore, the influence from the gas phase turbulence on the 100 μm particle trajectories is negligible in comparison with the influence from the wall roughness as shown in Figure 6.12(b) and 6.12(c).

To further investigate the effects of wall roughness on the particle trajectories, 58 particles with streamwise velocity of 10 m/s were released from line A as shown in Figure 6.11 (y = 0.276m), which is located 1D upstream from the bend entrance. Figure 6.13(a), (b) and (c) show the particle trajectories in the bend for different wall roughness angles, i.e., 0°, 2.5° and 5°, respectively. With the increase of the wall roughness angle, the 'particle free zone' occurring at the inner wall region is reduced as the wall roughness increases. For the 5° case, particles were found to disperse further into the upper region of the channel after the bend, following the first collision. This same region is observed to be a 'particle free zone' for the 0° case.

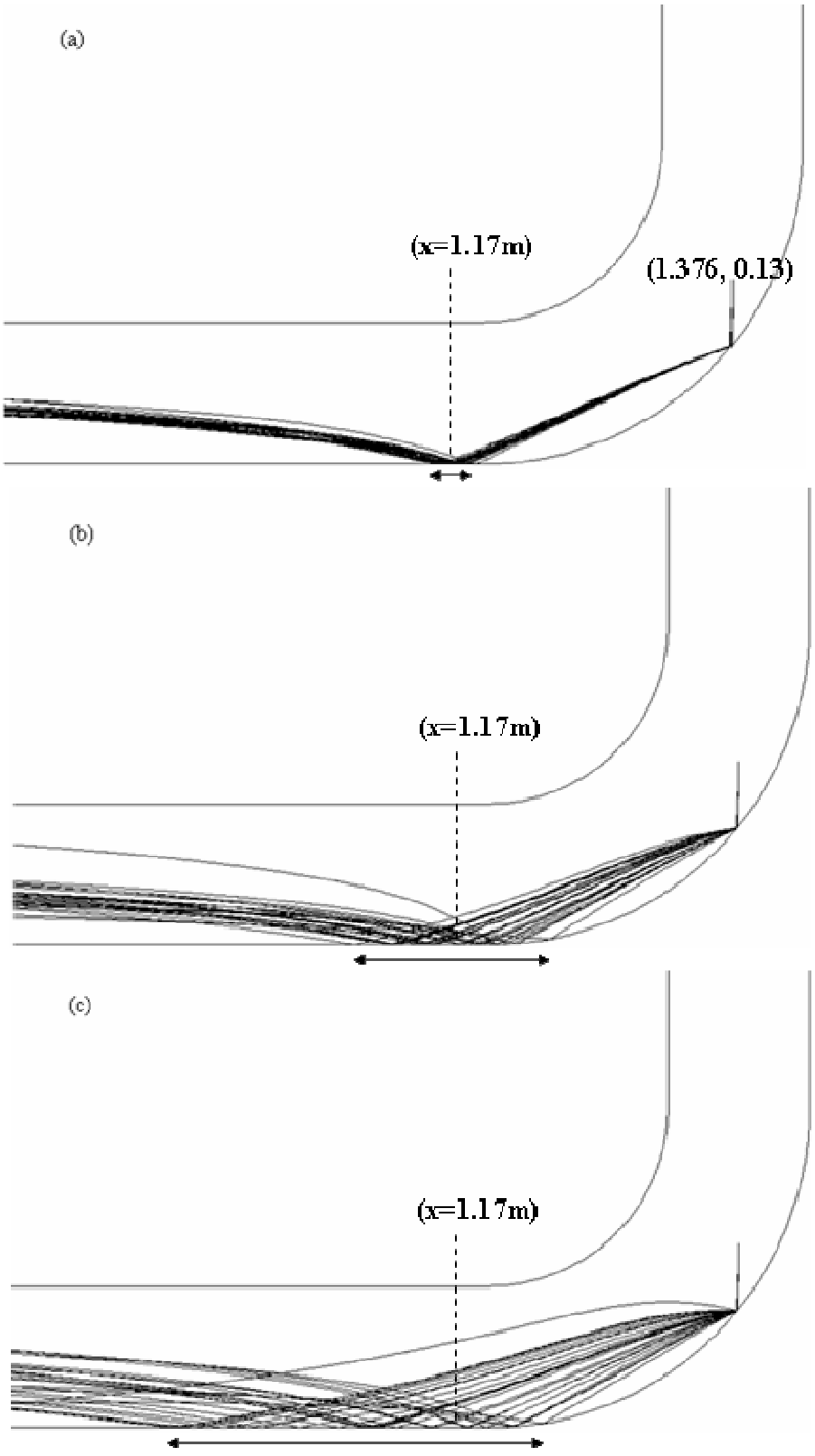

Figure 6.12 Computed trajectories for 100 μm particles released with different wall roughness angle: (a) 0°, (b) 2.5° and (c) 5°. ◄⟶► The length of the second collision region.

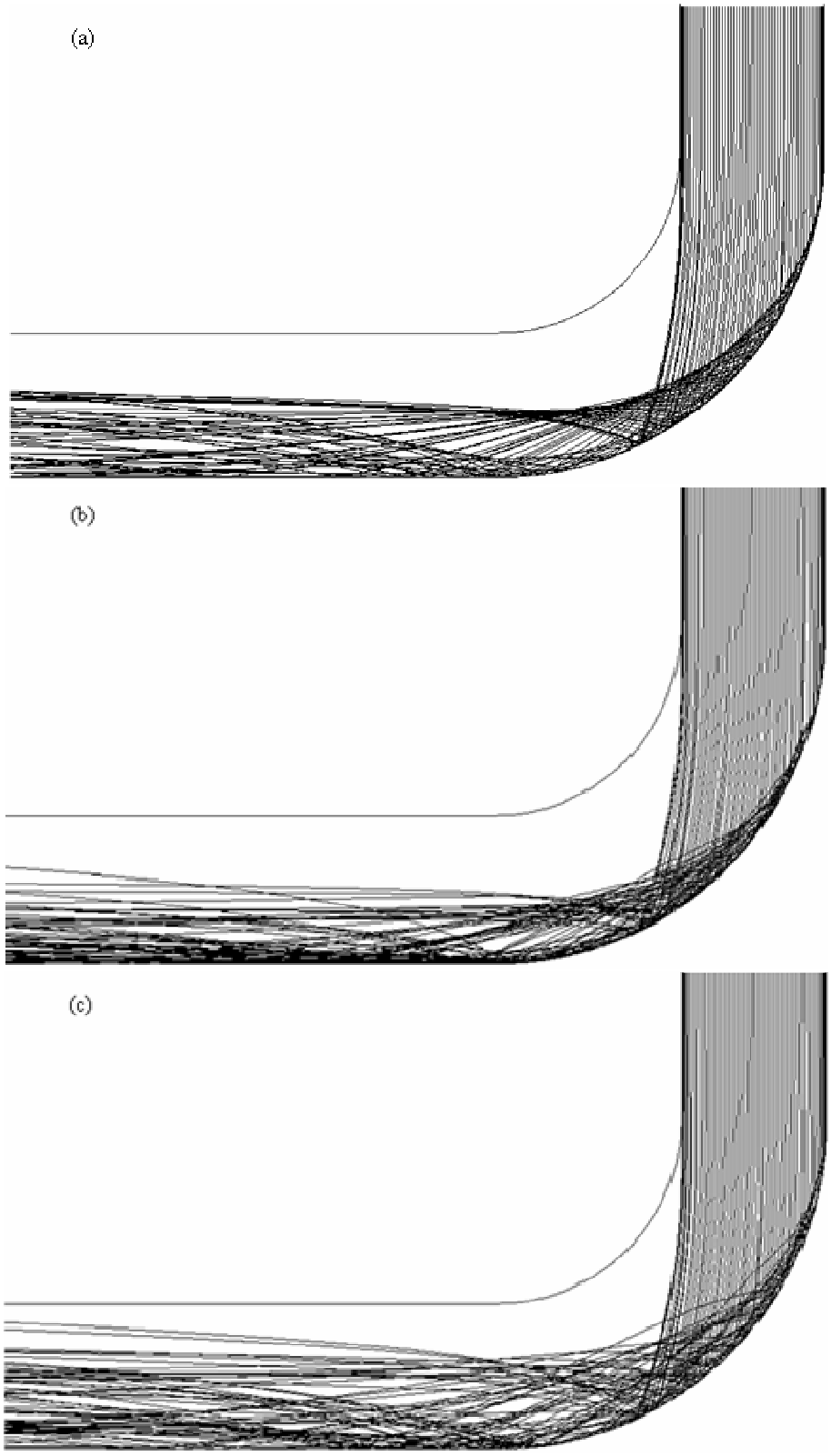

Figure 6.13 Computed trajectories for 100 μm particles released 0.1m before the bend with different wall roughness angle: (a) 0°, (b) 2.5° and (c) 5°.

6.2.4 The effects of wall-roughness on particle number density

To investigate the influence of wall roughness on the particle dispersion, the particle number density distribution taken along different sections around the bend is used. To obtain statistically meaningful results a larger number of particles is now used where 100,000 mono-sized particles (100μm) with streamwise velocity of 10 m/s were released from 100 uniformly distributed points across line A (Figure 6.11). The independence of statistical particle phase prediction from the increase of the number of particles used was tested by implementing 50,000, 100,000 and 200,000 particles. The difference of the particle phase velocities at θ=0° of 50,000 and 100,000 particles was less than 3 % and for 100,000 to 200,000 was less than 1%, thus in terms of computational efficiency 100,000 particles was used hereafter.

The particle number density normalised by the number of inlet particles, 100, 000 at θ= 30° with different wall roughness angles, are presented in Figure 6.14(a). The particle distribution profiles in this case for the three wall roughness angles are very similar. A much higher particle number density for all roughness angles is found near the outer wall region and this phenomenon is consistent with the observations from the experimental study of Kliafas and Holt (1987) and the Eulerian-Eulerian simulation of Tu and Fletcher (1995). In Figure 6.14(b), with the turning of the bend from θ= 30° to θ= 60° the trend for particle number density sees an increase in the outer region from r*=0.65 to r*=0.9 for all wall roughness angles and a decrease in the region from r*=0.4 to r*=0.45 for roughness angle of 5°. No particles are found in the inner wall region (from r*=0 to r*=0.4). This is due to the high inertia of 100 μm particles, which causes particles to respond slowly to the local gas phase changes. At θ= 60°, an interesting phenomenon is found for the 0° wall roughness case where two local maximus for particle number density are observed at the region at r* = 0.75 and in the outer wall region. The prediction of high particle number density in the middle bend region was not found either in the experimental study of Kliafas and Holt (1987) or the Eulerian-Eulerian simulation of Tu and Fletcher (1995). This non-physical phenomenon is remedied when the wall roughness is taken into consideration. The high particle number density at r* = 0.75 is reduced dramatically when the wall roughness was increased to 2.5°. A further increase to 5°, showed a smoother particle number density profile, suggesting a greater dispersion of particles being distributed over a

greater area within the bend. This leads to a significant decrease in the 'particle free zone'. However, the total number of particles in the region from r*=0.4 to r*=0.55 is about 2000 which accounts for 2% of the total particles tracked whereas high particle number densities are found in the region next to the outer wall for all roughness angles. A similar phenomenon is found at θ= 90° in Figure 6.14(c), the high particle number density at r*=0.6 is found in the 0° wall roughness case. With the increase of wall roughness angles, the high particle density at this region is dramatically reduced. Figure 6.14(d) shows the particle distribution profiles at Line B, 1D after the exit. It is seen that the wall roughness structure enhances the re-dispersion of particles after the first collision leading to the smoother particle number density profile. Additionally, the 'particle free zone' was reduced with an increase in the wall roughness and relatively low particle number densities were observed in the region from r*=0.25 to r*=0.32.

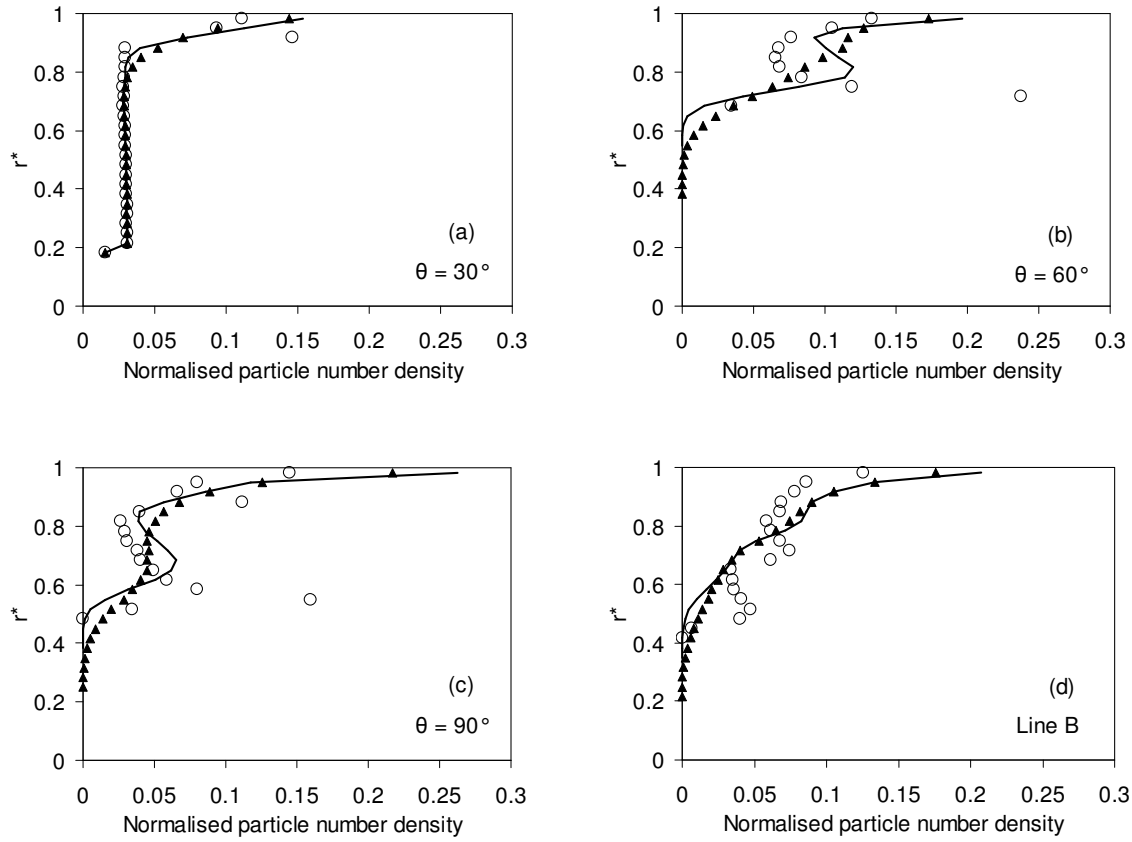

Figure 6.14 Computed particle number concentration with different wall roughness angles at different locations. Circles: 0° roughness, Line: 2.5° roughness, Solid triangle: 5° roughness.

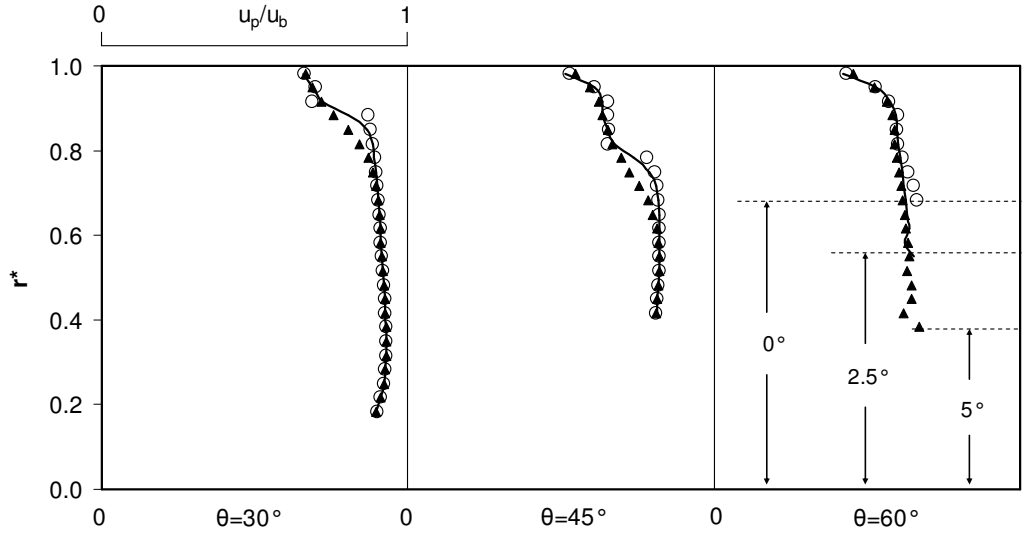

(a)

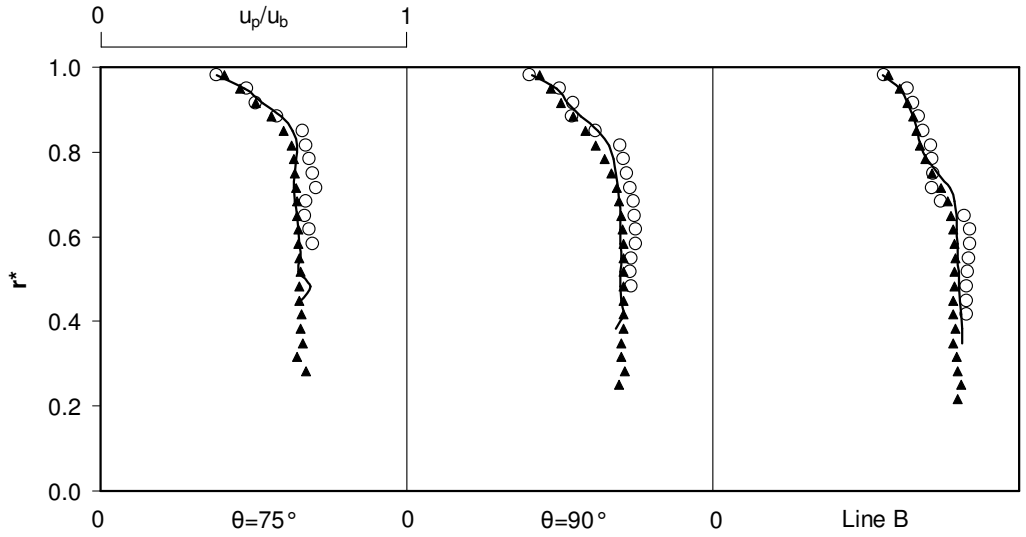

(b)

Figure 6.15 Comparison of particle streamwise mean velocity profiles with different roughness angles at different locations. ⟷ The length of the particle free zone. Circles: 0° roughness, Line: 2.5° roughness, Solid triangle: 5° roughness.

6.2.5 The effects of wall-roughness on particle mean velocities

The effects of wall roughness on particle mean velocities at different locations in the bend are shown in Figure 6.15. At θ=30°, the streamwise velocity of 5° roughness is slightly smaller than the 0° case at the outer wall region from r* = 0.85 to r* = 0.92,. This is the consequence of particles having collided on the outer wall before 30° and the loss of

momentum which is greater for walls with a higher roughness. However, the particle streamwise velocity profiles for the rest of the region is almost identical for all wall roughness, since this region is still in the early stages of the bend and particle collision has not occurred.. After θ=60°, however, the bend curvature is much greater and most particles have experienced the first wall collision resulting in a reduction in the mean streamwise velocities due to the average increase in momentum loss. This can be seen in the comparison of velocity profiles for at θ= 0^o to at θ= 60^o which has shifted to the left. For bend angles, θ > 60^o the mean velocity profiles for 0^o wall roughness exhibit larger magnitudes than for 2.5^o and 5^o wall roughness. The higher wall roughness causes the particles to lose more of its momentum whilst dispersing the particles in greater directions, hence the wider velocity profile, reaching to r* = 0.2 (from the outer wall r*=1) for 5^o roughness, compared with r* = 0.4 for 0^o roughness at Line B.

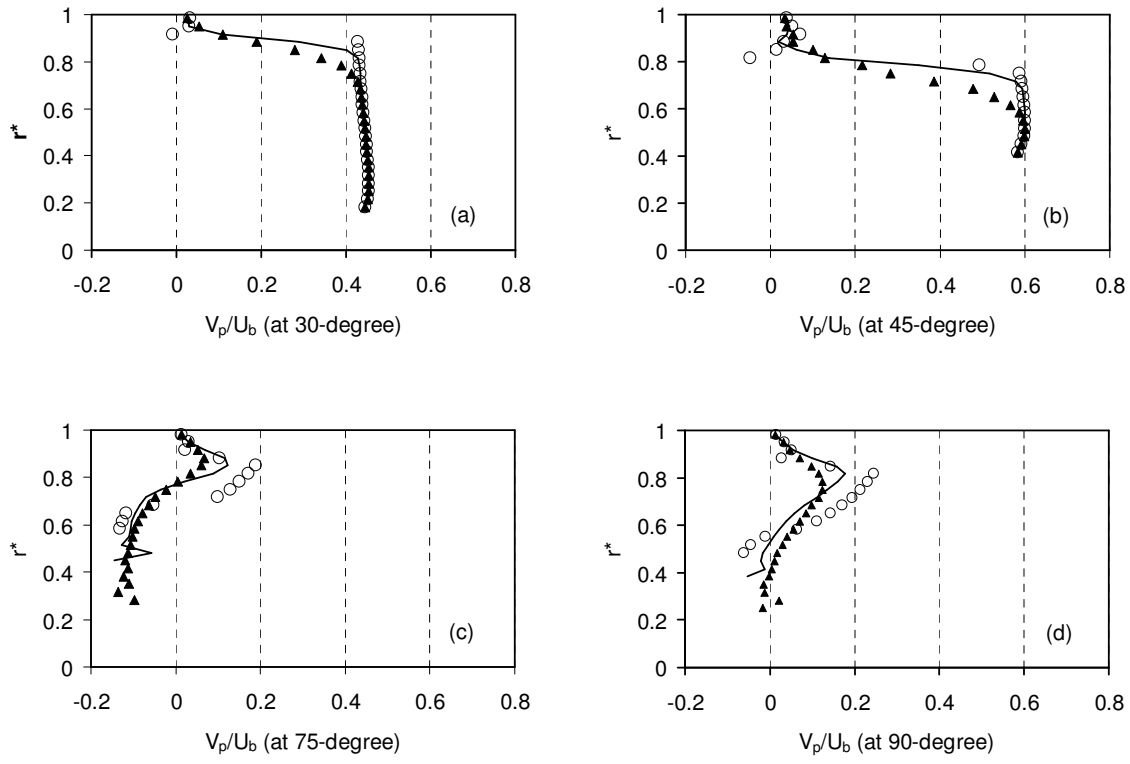

Figure 6.16 Comparison of particle transverse mean velocity profiles with different roughness angles at different locations. Circles: 0° roughness, Line: 2.5° roughness, Solid triangle: 5° roughness.

Figure 6.16 shows the particle mean transverse velocities at different locations. At θ=30°, the velocity profiles for different wall roughness angles are almost identical except for the region from r* = 0.85 to r* = 0.92. At θ= 45°, the velocity profile for 5° roughness is much

smaller than the 0° roughness profile at the region from r* = 0.62 to r* = 0.79. At θ=75°, the mean transverse velocities of 2.5° and 5° roughness are identical and slightly smaller than the smooth wall case. This can be attributed to the early collision occurring before θ=45°. The reduction of this particle mean velocity is consistent with observations that wall roughness reduces the mean particle velocities as obtained by Kussin and Sommerfeld (2002) and Benson et al. (2006).

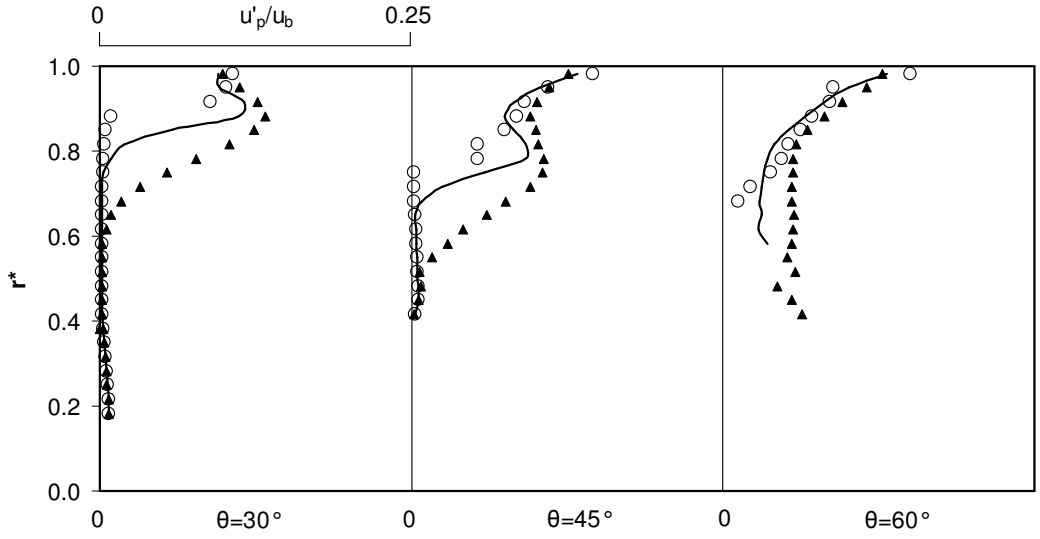

(a)

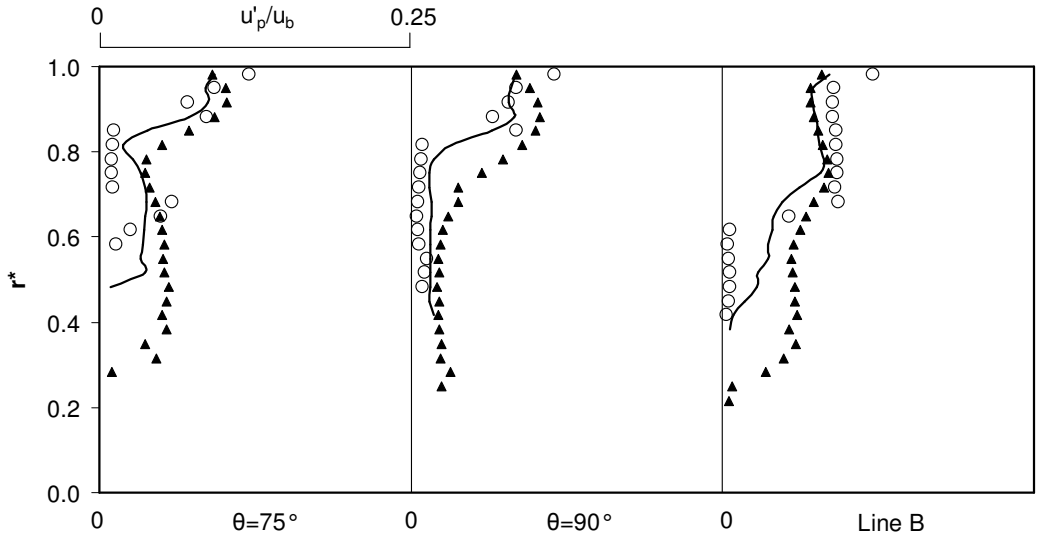

(b)

Figure 6.17 Comparison of particle streamwise fluctuating velocity profiles with different roughness angles at different locations.

6.2.6 Effects of wall-roughness on particle fluctuating velocities

Figure 6.17 illustrates the distribution of the particle streamwise fluctuating velocities for 0°, 2.5° and 5° roughness angles at various locations. As shown in Figure 9a, the particle velocity fluctuations at θ= 30° for all three roughness angles yielded almost zero turbulence intensities from r*= 0.2 to r* = 0.62. This is attributed to the fact that particle fluctuating velocity is zero at the inlet (Line A) and most particles flowing through this region have not collided with the bend yet. Considerably higher particle velocity fluctuations were found in the region near the outer wall to r* = 0.62 which is a result of the particle collisions at outer wall. Also, the particle streamwise fluctuating velocities of 2.5° and 5° roughness angles are higher than the 0° case, since the wall roughness model enhances the randomness for particle velocities and trajectories after collision. At θ= 45°, the particle streamwise fluctuating velocities of 2.5° and 5° roughness angles are higher than the 0° case from r*=0.5 to r*=0.9.

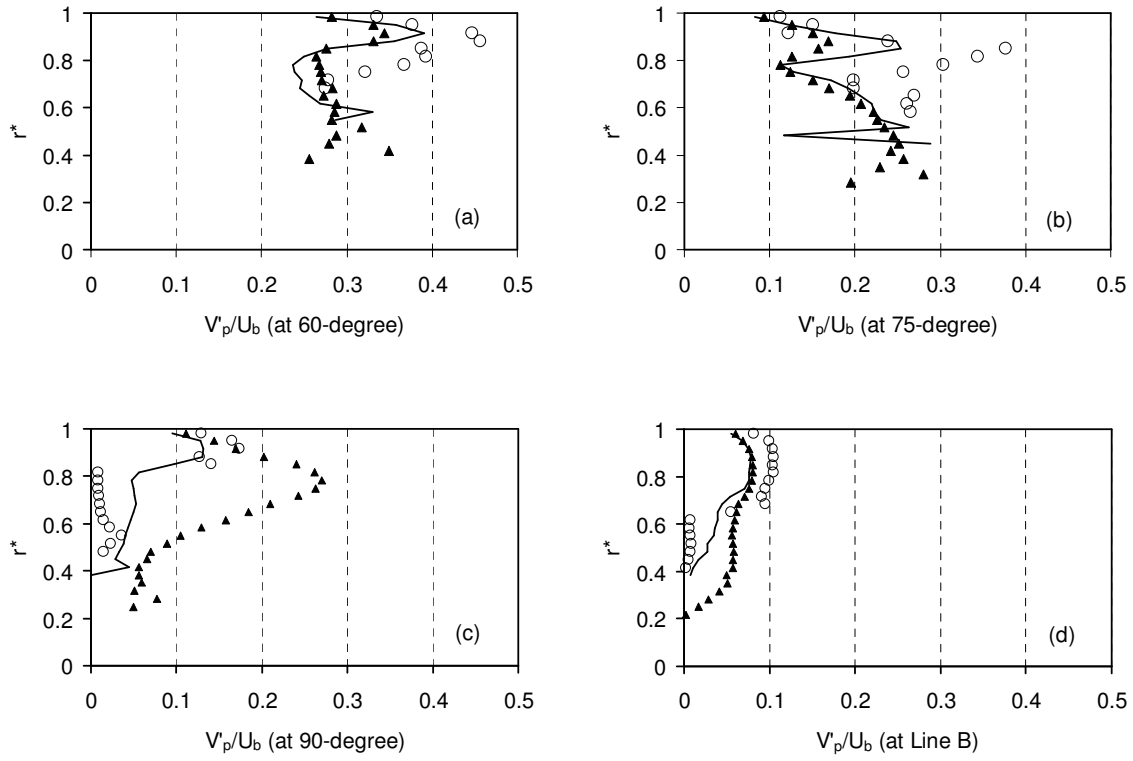

Figure 6.18 Comparison of particle transverse fluctuating velocity profiles with different roughness angles at different locations.

The particle transverse fluctuating velocities with different wall roughness angles are shown in Figure 6.18. An interesting phenomenon can be seen at θ= 60° where the transverse fluctuating velocities for all wall roughness cases are high. This is due to the dominant particle collision which produces a particle rebound velocity that is slightly smaller than the incident velocity due to the momentum lost during the collision process. At θ= 90°, the particle transverse fluctuating velocities of 2.5° and 5° roughness angles are higher than the smooth wall case. Figure 6.17 and 6.18 clearly indicate that the wall roughness has a significant influence on the particle velocity fluctuations.

6.2.7 Summary

The physical behaviors of a dilute gas-particle flow in a 90-degree bend were numerically investigated via a Lagrangian particle-tracking model. A substantial amount of work was taken in this study to elucidate further the understanding of the effect of wall roughness on the flow field of large particles (100 μm). It was found that the wall roughness considerably altered the rebounding behaviours of particles by significantly reducing the 'particle free zone' and smoothing the particle number density profiles. The numerical results confirmed that the particle mean velocities for 2.5° and 5° roughness angles were reduced due to the wall roughness which, on average increases the momentum loss for the particle phase. Also, the particle fluctuating velocities were increased when taking into consideration the wall roughness, since the wall roughness produced greater randomness in the particle rebound velocities and trajectories.